Pergamon

PII: S0191-8141(96)00113-7

Journal of Structural Geology, Vol. 19, Nos 3–4, pp. 369 to 381, 1997

0191-8141/97 $17.00 + 0.00

Geometries of syntectonic sediments associated with single-layer detachment folds

JOSEP POBLET

Departament de Geologia Dinàmica, Geofísica i Paleontologia, Facultat de Geologia, Universitat de Barcelona, C/Martí i Franquès s/n, 08071 Barcelona, Spain

KEN McCLAY

Fault Dynamics Project, Department of Geology, Royal Holloway University of London, Egham, Surrey TW20 0EX, U.K.

FABRIZIO STORTI

Dipartimento di Scienze Geologiche, Terza Università di Roma, Via Ostiense 169, 00154 Roma, Italy

and

JOSEP ANTON MUÑOZ

Departament de Geologia Dinàmica, Geofísica i Paleontologia, Facultat de Geologia, Universitat de Barcelona, C/Martí i Franquès s/n, 08071 Barcelona, Spain

(*Received* 8 *February* 1996; *accepted in revised form* 21 *October* 1996)

Abstract—Three kinematic models have been proposed to account for the geometry and kinematics of detachment folds involving a homogeneous competent layer detached over a ductile unit: Model 1 — variable limb dip–constant limb length, Model 2 — constant limb dip–variable limb length, and Model 3 — variable limb dip–variable limb length. Because the same fold shape can be generated by any of the above mechanisms, fold kinematics are best determined by the geometries of syntectonic sediments. In single-layer detachment folds, growth strata patterns are controlled by axial surface activity, limb rotation, limb lengthening, fold uplift rates, sedimentation rates and deformation mechanisms of the syntectonic sediments. Asymmetric kink folds have been modelled and compared with natural examples from the southern Spanish Pyrenees. Under conditions of high sedimentation rates, Model 1 folds produce characteristic fanning growth stratal wedges that initially onlap and then progressively overlap the detachment anticline, whereas at low sedimentation rates, anticlines with fanning growth wedges on both limbs are formed. Model 2 folds, under conditions of high syntectonic sedimentation rates, form anticlines with growth strata largely parallel to the pre-growth units and thinned over the fold crest. In contrast, at low sedimentation rates, Model 2 folds show offlapping growth strata onto both limbs. Model 3 growth folds, under conditions of high syntectonic sedimentation rates, form anticlines with intermediate features from Model 1 and Model 2; at low sedimentation rates, anticlines are formed with offlapping growth structures.

INTRODUCTION

Syntectonic sediment geometries have recently been recognised as a powerful tool which can be used to distinguish between different types of thrust-related folding (Suppe *et al.*, 1992; Hardy *et al.*, 1996). Growth strata act as a 'tectonic tape recorder' in that they can provide a record of the deformation kinematics and progressive development of thrust fault-related folding. The geometries of growth strata associated with fault-bend and fault-propagation folds have received much attention (Suppe *et al.*, 1992; Hardy and Poblet, 1995), but there has been little equivalent modelling of detachment folds. Hardy and Poblet (1994) have analysed growth strata associated with a single limb of a constant limb length detachment fold and Torrente and Kligfield (1995) examined low amplitude buckle folds with associated growth strata. Detachment folds with growth strata can form in foldbelts and thrust systems which develop in regions with active sedimentation both in marine basins (cf. Gulf of Mexico — Rowan *et al.*, 1993, Apennines — Torrente and Kligfield, 1995 and the Pyrenees — Poblet and Hardy, 1995) and in non-marine environments (cf. Pyrenees — Burbank and Vergés, 1994).

Detachment folding occurs where the displacement related to a layer-parallel blind thrust is accommodated by folding in the hangingwall (Jamison, 1987). Three different kinematic models have been proposed for detachment folds where a homogeneous competent unit with competent bed length and thickness is detached over a ductile unit (Fig. 1) (Homza and Wallace, 1995; Poblet and McClay, 1996). These are: (a) anticlines formed with variable limb dip and constant limb length (Fig. 1a) (De

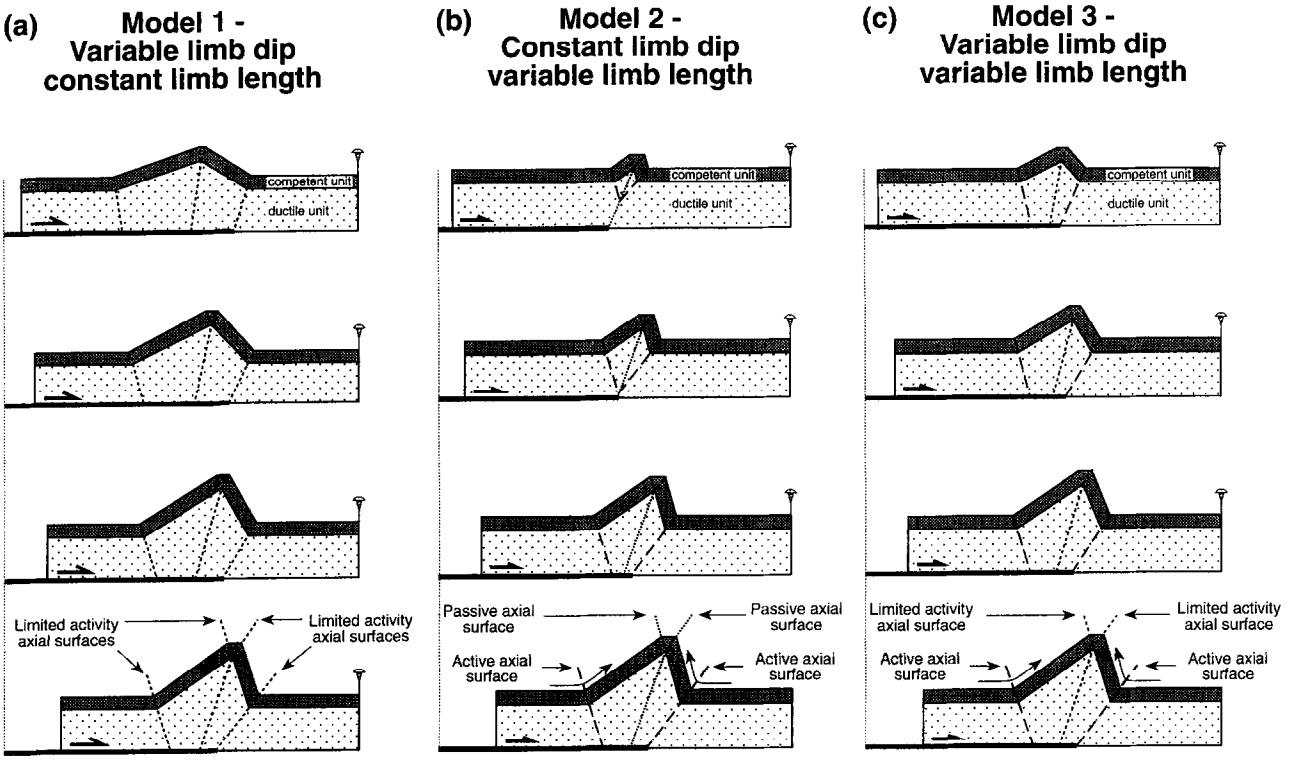

Fig. 1. Evolution of three different models for asymmetric kink detachment folds involving a homogeneous competent layer detached over a ductile unit. The models are calculated using the parameters given in Table 1 and all three kinematic models produce the same final fold shape. All the models are area balanced for both the competent and ductile units. In the case of Models 1 and 2 variations in the depth to detachment occur in order to area balance the ductile unit (Homza and Wallace, 1995).

Sitter, 1956), (b) anticlines developed with constant limb dip and variable limb length (Fig. 1b) (Mitchell and Woodward, 1988), and (c) anticlines developed with variable limb dip and variable limb length (Fig. 1c) (e.g. Dahlstrom, 1990).

In this paper we model the development of single layer, asymmetric detachment folds with the addition of syntectonic growth strata and compare the resultant geometries with natural examples of detachment growth folds from the southern Spanish Pyrenees. Three different detachment fold types (Fig. 1) are modelled using the fold parameters summarised in Table 1. Results of models formed under conditions of high syntectonic sedimentation (covered anticlines) and low syntectonic sedimentation (emergent anticlines) are presented as well as models where the growth strata have been deformed by flexural slip, shear parallel to the pre-growth beds or by vertical shear.

Table 1. Geometrical parameters of the final detachment fold stage, and thrust slip and sedimentary rates used for modelling detachment growth folds

	Detachment fold
Backlimb dip	35°
Forelimb dip	74°
Backlimb length	10 units
Forelimb length	6 units
Backlimb length/ forelimb length	1.6
Slip	6 units
Uplift	5.8 units
Interlimb angle	71°
Axial plane dip	70°
Depth to detachment	4.6 units
Thickness of the competent unit	1.5 units
Ductile unit thickness/competent unit thickness	3.0
Slip rate	1.5 units/stage
Syntectonic sediment rate (high sedimentation rate)	2.1 units/stage
Syntectonic sediment thickness (low sedimentation rate)	1.0 units/stage

GEOMETRIC MODELS OF DETACHMENT FOLDS

The three principal kinematic models for the progressive development of single layer detachment folds are summarised in Fig. 1. The progressive evolution of these three detachment fold models (1–3) has been calculated using the equations presented in Poblet and McClay (1996) and display four equal increments of 1.5 units of shortening (Fig. 1). In the variable limb dip and constant limb length detachment folding (Model 1, Fig. 1a) folding and shortening occur mainly by limb rotation. The axial surfaces rotate to maintain constant stratigraphic thickness and the fold widths decrease. In contrast, constant limb dip and variable limb length detachment folding (Model 2, Fig. 1b) is a self-similar mechanism where folds grow exclusively by axial surface migration. The folds nucleate instantaneously as small width structures with fixed limb dips and axial surface dips, and fold boundaries migrate outwards to accommodate continued shortening. Fold width increases as shortening progresses. In variable limb dip and variable limb length detachment folding (Model 3, Fig. 1c), both axial surface migration and limb rotation take place. These folds nucleate as narrow folds and shortening is accommodated by both outward migration of the axial surfaces and limb rotation. As in Model 1, the axial surfaces rotate to maintain constant stratigraphic thickness.

The three kinematic models for the progressive evolution of detachment folds give different evolutionary paths in terms of rates of uplift, rates of limb rotation and rates of limb lengthening (Fig. 2). All curves displayed in the graphs converge to a common end point indicating that the same final fold geometry is generated by each kinematic model. In the cases where limb rotation occurs (Models 1 and 3) both uplift and limb dip increase rapidly in the first stages and then increase almost linearly but at slower rates (Fig. 2a–c). In Model 2 detachment folds uplift increases linearly (Fig. 2a) and limb dip is constant with increased shortening (Fig. 2b & c). Limb length increases linearly in Model 2 folds, whereas for Model 3 it increases rapidly in early stages of fold growth and more slowly in later stages (Fig. 2d & e).

Figure 1 also illustrates the axial surface activity in the different models. Three types of axial surfaces can be distinguished in detachment folds: (a) passive axial surfaces which are transported together with the rocks (Suppe *et al.*, 1992), (b) limited activity axial surfaces which are pinned to the base of the competent unit so that a restricted amount of strata rolls through the axial surfaces due to the rotation of the axial surfaces (Poblet and McClay, 1996), and (c) active axial surfaces through which material passes freely (Suppe *et al.*, 1992). In Models 1 and 3 all axial surfaces progressively rotate with increasing shortening in order to keep constant stratigraphic thicknesses, resulting in slight widening of the flat anticlinal crest. In Model 2 the dips of axial surfaces remain constant and consequently the flat crest width also stays constant.

These three kinematic models for detachment folds can produce identical final fold shapes (Fig. 1) and hence the finite fold geometry as displayed by the pre-kinematic strata is not sufficient in itself to determine which kinematic mechanism formed a particular fold. Recognition of hinge migration ('rolling hinges') by use of variations in patterns of fibre curvature in syntectonic pressure shadows (e.g. Beutner and Diegel, 1985), and microstructures (fabrics and fractures) (Fischer *et al.*, 1992) may possibly rule out the constant limb length detachment fold model (Model 1), where hinge migration does not occur, but hinge migration may not always be possible to identify nor would it permit distinction between Models 2 and 3. Growth stratal architectures, however, may show different patterns according to different kinematic models of detachment fold formation. In this paper we use the fundamental detachment fold models as presented in Poblet and McClay (1996) (Fig. 1) with the addition of simple synkinematic sedimentary sequences to illustrate how different detachment fold kinematics generate different growth stratal architectures.

DETACHMENT GROWTH FOLD MODELS

Asymmetric kink detachment growth folds formed with constant shortening rates have been modelled using the three principal kinematic mechanisms outlined above and illustrated in Fig. 1. The finite fold geometries as shown by the pre-growth strata are identical in all of the models and summarised in Table 1. Two scenarios have been simulated: (a) constant high sedimentation rate where the growth strata essentially cover the growing anticline — uplift rate less than sedimentation rate, and (b) constant low sedimentation rate where the fold uplift rate is greater than the sedimentation rate such that the anticlines remain emergent. This syntectonic sedimentation consisting of simple flat-lying sediments without any syntectonic erosion and redeposition (on slopes or in the adjacent basins) has been added to each of the four deformation increments of the folds shown in Fig. 1. The models are incremental with the anticlines frozen at each step and with the growth sediments added instantaneously to the flanks/crest. Compaction has not been considered in our simple models. Growth stratal architectures are controlled by fold kinematics, relative uplift rates (Fig. 2a) and relative sedimentation rates. Figures 3–8 show the results of detachment growth folds modelled where the internal deformation mechanism is essentially flexural slip with constant bed length and where the growth strata load has no effect on the deformation rates. Figures 9–12 show the additional effects of changing the deformation in the growth strata such that they are internally deformed either by shear

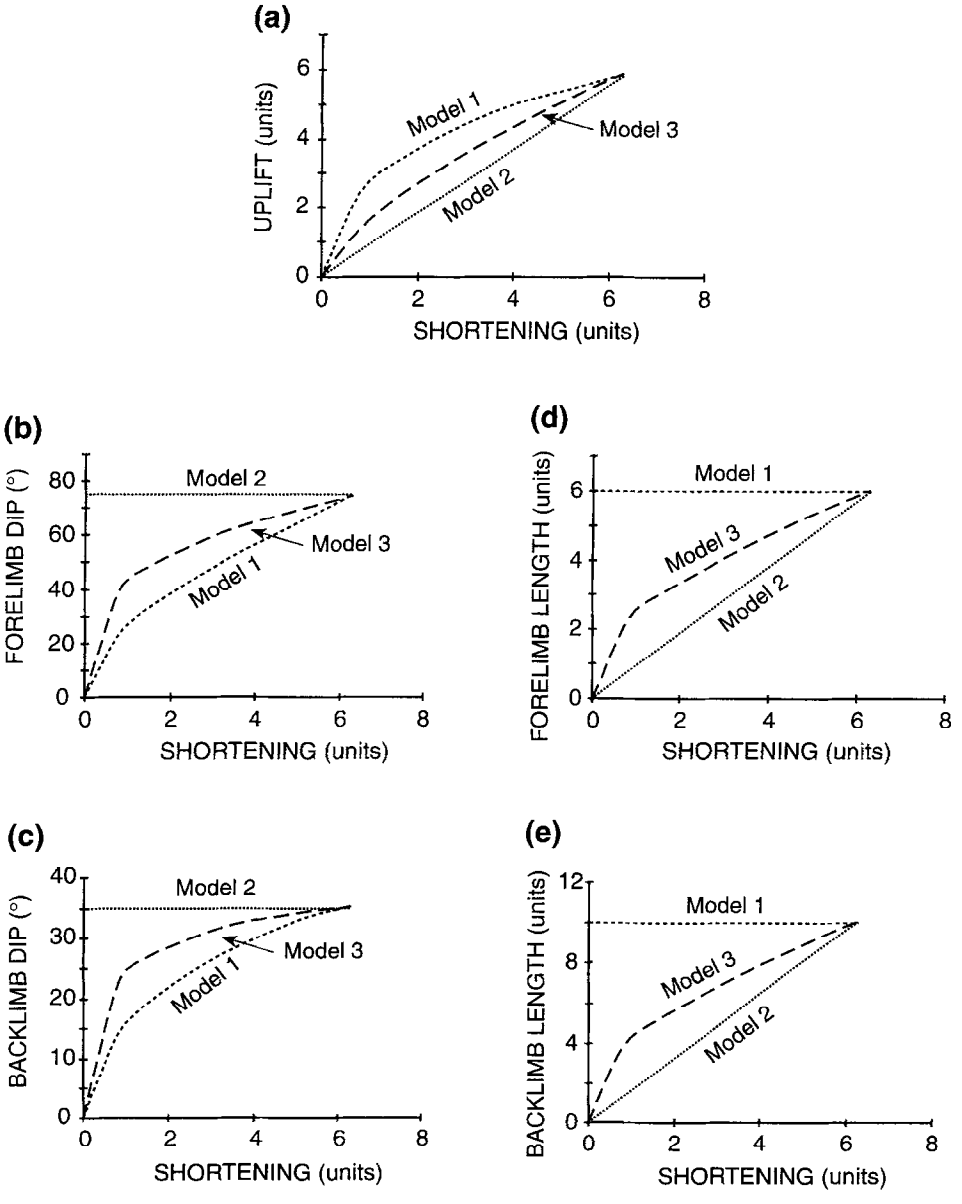

Fig. 2. Graphs of uplift, limb dip and limb length versus shortening for detachment folds having the same final fold geometry and modelled using the parameters in Table 1. The length units can be any unit of distance.

parallel to the pre-growth beds or by vertical simple shear.

Covered anticlines — high sedimentation rate (deformation of growth strata by flexural slip)

Covered anticlines form where the sedimentation rate is high such that for most of the fold history it is buried (Figs 3–5). In Models 1 and 3 (Figs 3 & 5) the early stages of contraction give slightly emergent detachment anticlines because of faster uplift rates (Fig. 2a), whereas Model 2 anticlines (Fig. 4) remain covered throughout their deformation history as a result of the constant uplift rate (Fig. 2a). Growth stratal architectures are different for each of the three kinematic mechanisms modelled.

Model 1 — constant limb length–variable limb dip. Model 1 detachment folds with high syntectonic sedimentation rates produce growth anticlines that show onlapping synkinematic stratal architectures on both forelimb and backlimb in the first two increments of deformation (Fig. 3). In the last two stages a syncline is developed in the growth strata overlapping the anticlinal crest. On both limbs growth stratal dip decreases upsection. The final growth fold geometry shows different growth stratal patterns on the two limbs because of different rates of limb rotation (Fig. 2b & c), thereby indicating the asymmetry and vergence of the detachment fold.

Model 2 — constant limb dip–variable limb length. In Model 2 detachment folds the growth strata do not onlap

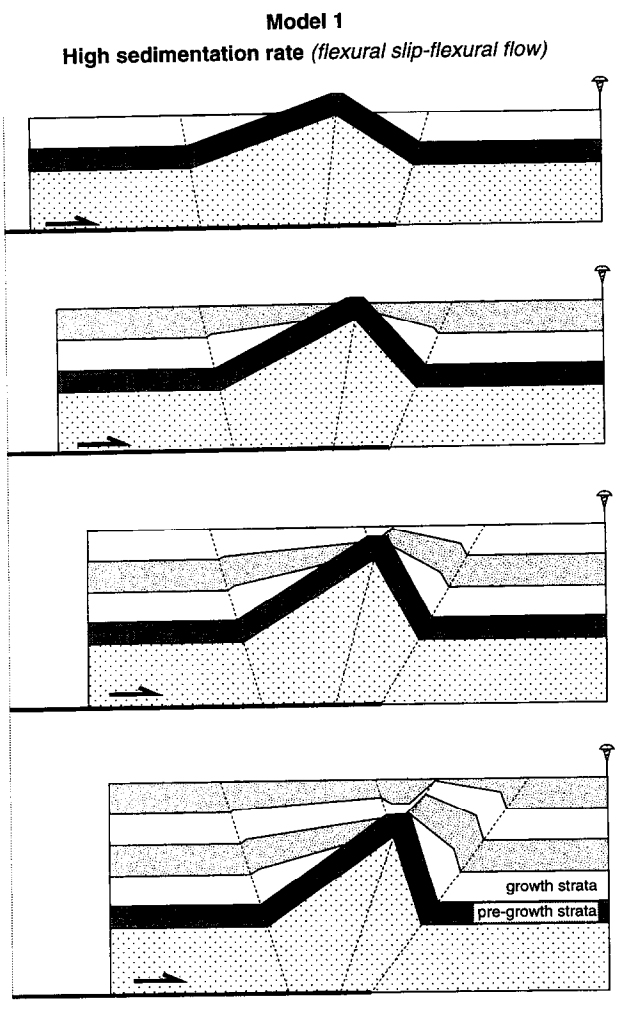

Fig. 3. Model 1 detachment growth folds showing four successive stages of shortening with uplift rate lower than sedimentation rate except for the first two stages (model parameters are given in Table 1). Growth strata are deformed by flexural slip–flexural flow.

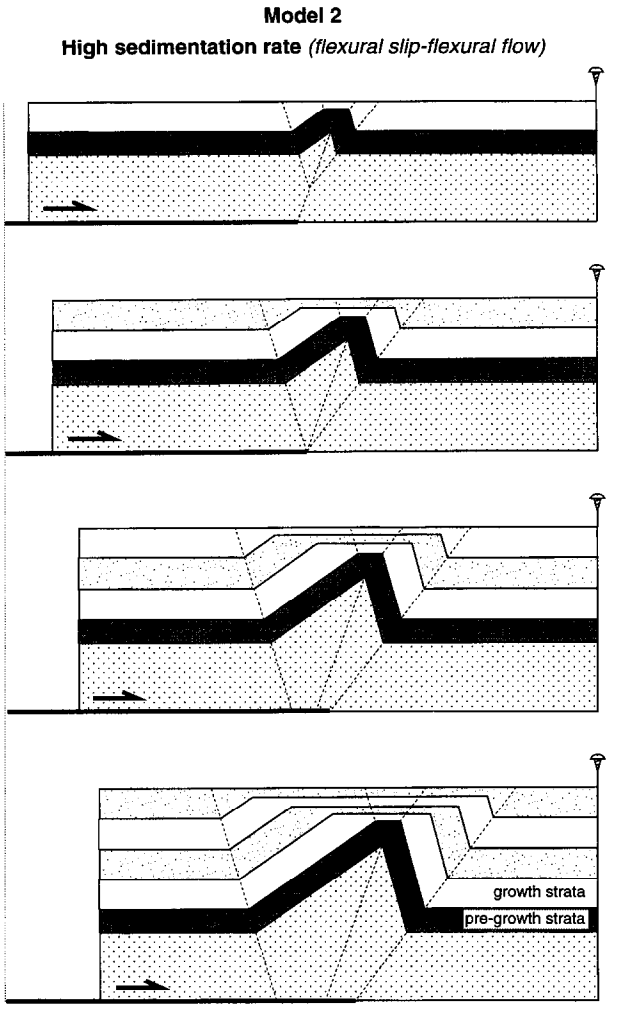

Fig. 4. Model 2 detachment growth folds showing four successive stages of shortening with uplift rate lower than sedimentation rate (model parameters are given in Table 1). The growth strata are deformed by flexural slip–flexural flow.

either the backlimb or the forelimb but merely thin systematically over the crest of the growing anticline (Fig. 4), and they are largely parallel to the pre-growth strata.

Model 3 — variable limb length–variable limb dip. Because there are a number of generalities related to the kinematics/growth stratal geometries apparent in Models 1 and 2 that can be applied to Model 3, this model will be described by analogy with Models 1 and 2 without showing all the incremental stages. In Model 3 detachment folds, growth strata have geometries intermediate between Models 1 and 2 (Fig. 5); old growth strata onlapping the limbs, asymmetric pattern, slight fan geometry of the growth strata in the upper part of the fold limbs and low amplitude crestal syncline as in Model 1, but much of the growth strata in the lower part of the fold limbs are parallel to the pre-growth units as in Model 2.

Emergent anticlines — low sedimentation rate (deformation of growth strata by flexural slip)

Emergent anticlines form where the sedimentation rate is low relative to the fold uplift rate such that the fold

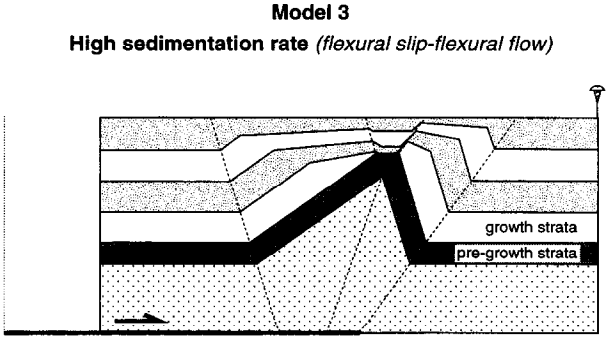

Fig. 5. Model 3 detachment growth fold showing the last stage of shortening with uplift rate lower than sedimentation rate except for the first stage (model parameters are given in Table 1). Growth strata are deformed by flexural slip–flexural flow.

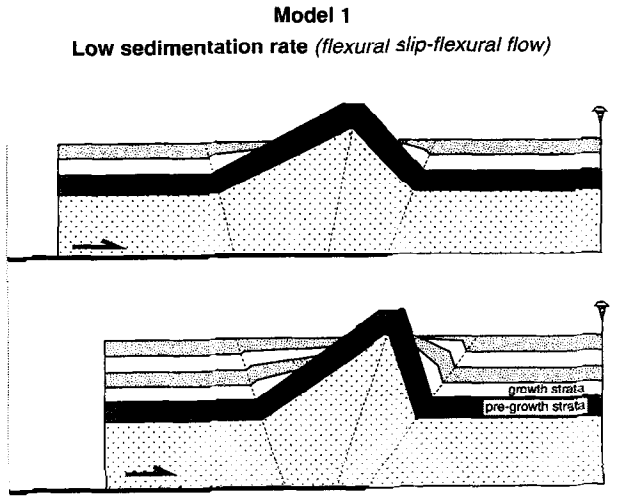

Fig. 6. Model 1 detachment growth folds showing two stages of shortening with uplift rate greater than sedimentation rate (model parameters are given in Table 1). Growth strata are deformed by flexural slip–flexural flow. Stages shown are for slip increments of 3 and 6 units.

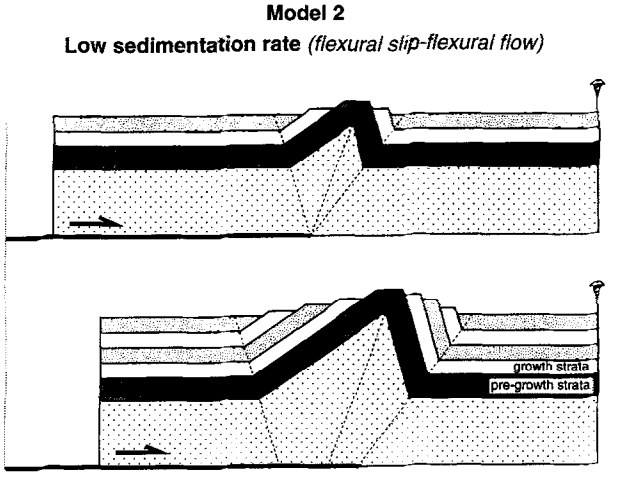

Fig. 7. Model 2 detachment growth folds showing two stages of shortening with uplift rate greater than sedimentation rate (model parameters are given in Table 1). Growth strata are deformed by flexural slip–flexural flow. Stages shown are for slip increments of 3 and 6 units.

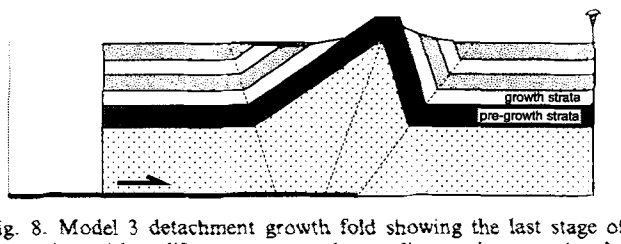

Fig. 8. Model 3 detachment growth fold showing the last stage of shortening with uplift rate greater than sedimentation rate (model parameters are given in Table 1). Growth strata are deformed by flexural slip–flexural flow.

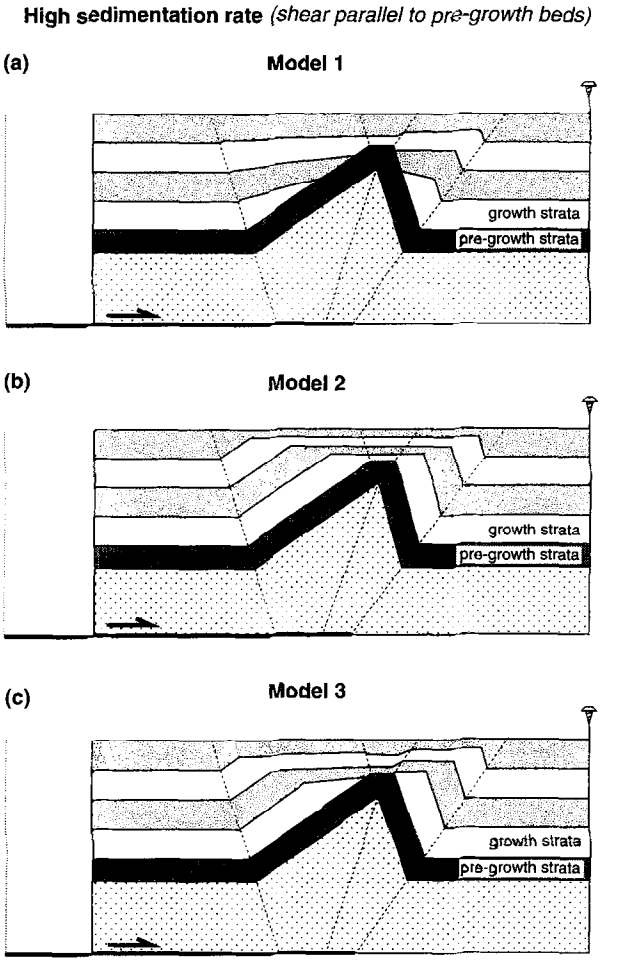

Fig. 9. Forward modelled growth detachment folds for uplift rate lower than sedimentation rate except for the initial stages in (a) and (c) (model parameters are given in Table 1). Growth strata are deformed by shear parallel to pre-growth beds. Only the final stages are shown.

crest remains emergent throughout the fold's history (Figs 6–8). In the emergent fold models presented in this paper a simplistic situation of no erosion of the fold crest is modelled. As in the case of high sedimentation rate models, growth stratal architectures are different for each of the three kinematic mechanisms modelled.

Model 1 — constant limb length–variable limb dip. Model 1 detachment folds with low syntectonic sedimentation rates produce growth anticlines that show onlapping synkinematic stratal architectures on the backlimb, whereas forelimb growth strata initially onlap and then offlap the anticline (Fig. 6). Growth strata progressively decrease in dip up-section. The different growth stratal patterns on both limbs indicate the asymmetry and vergence of the detachment fold.

Model 2 — constant limb dip–variable limb length. In Model 2 detachment folds the first syntectonic growth package onlaps both limbs but subsequently deposited units show successive offlapping configurations as

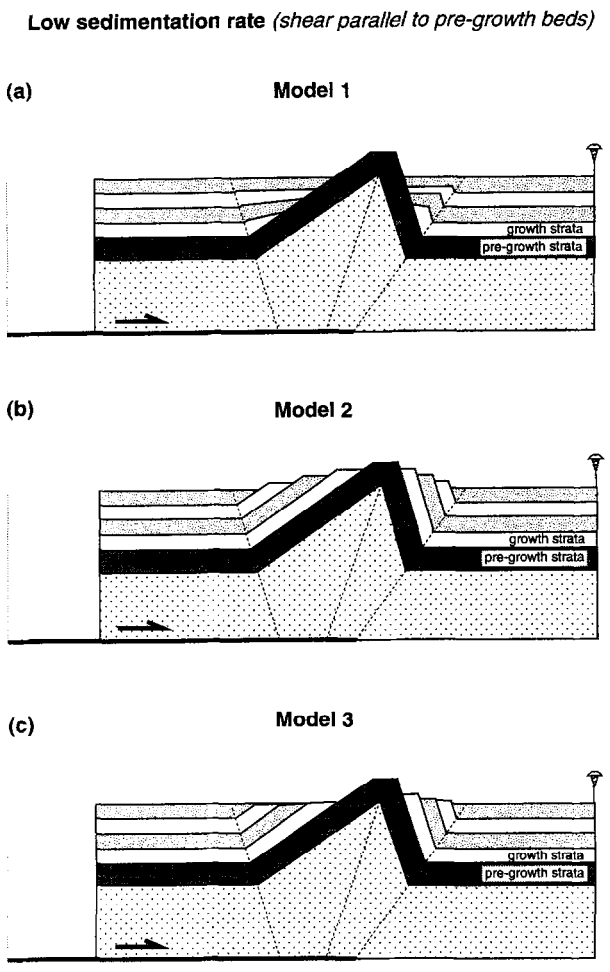

Fig. 10. Forward modelled growth detachment folds for uplift rate greater than sedimentation rate (model parameters are given in Table 1). Growth strata are deformed by shear parallel to pre-growth beds. Only the final stages are shown.

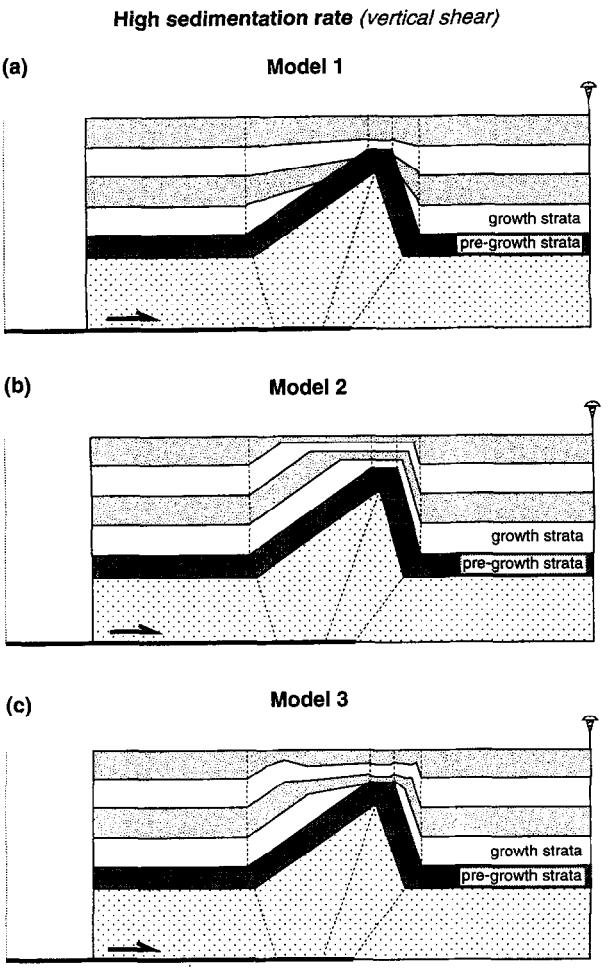

Fig. 11. Forward modelled growth detachment folds for uplift rate lower than sedimentation rate except for the initial stages in (a) and (c) (model parameters are given in Table 1). Growth strata are deformed by vertical simple shear. Only the final stages are shown.

previously deposited units are uplifted by the growing anticline (Fig. 7).

Model 3 — variable limb length–variable limb dip. In Model 3 detachment folds the growth strata geometry is very similar to Model 2 folds (Fig. 8). Growth strata onlap both limbs, but with increased shortening, backlimb growth strata develop offlap geometries that become less significant as the uplift rate decreases with shortening, whereas forelimb sediments develop simple offlap geometries. An asymmetric anticline and growth stratal pattern is developed but there are only subtle and relatively minor differences between forelimb and backlimb geometries.

Deformation of growth strata by shear parallel to pre-growth beds

Growth strata geometries in detachment folds can also be affected by the deformation mechanisms operating as the fold forms. The models described above were all generated by flexural slip deformation in both the pre-growth and growth strata. If the anisotropy in growth strata is weak to non-existent it is possible that they may deform by shear parallel to the pre-growth units. Such a case is shown in Fig. 9 for detachment folding with high sedimentation rates. Minor variations in the dips of growth strata are found on the forelimbs of Model 1 and Model 3 folds and there is a decrease in the amplitude of the syncline at the fold crest in Model 1 and Model 3 folds. In models with low sedimentation rates there is only discernible differences in Model 1 with no offlap in the forelimb strata as compared with simulations where the growth strata are deformed by flexural slip (Fig. 10). In all cases the growth stratal architectures are almost identical to those produced where the deformation mechanism is flexural slip in the growth units.

Deformation of growth strata by vertical simple shear

Figures 11 and 12 show the results of modelling detachment growth folds where the growth strata are

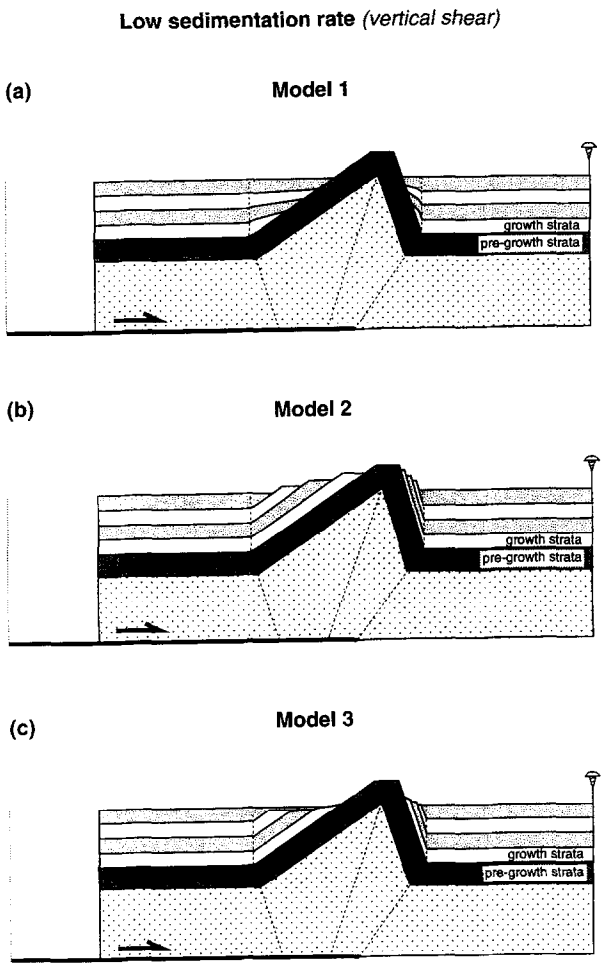

Fig. 12. Forward modelled growth detachment folds for uplift rate greater than sedimentation rate (model parameters are given in Table 1). Growth strata are deformed by vertical simple shear. Only the final stages are shown.

deformed by vertical simple shear, perhaps simulating deformation of weak, unconsolidated synkinematic sediments. In these models the finite growth stratal architectures are significantly different from those generated by flexural slip deformation. In particular, the thickness of the forelimb growth strata is substantially decreased. In Models 1 and 3 the dips of the forelimb growth wedge are markedly increased, whereas the dips of backlimb growth strata are only mildly increased. In the case of high sedimentation rate the development of a growth syncline on the crest of the detachment anticline in Models 1 and 3 is significantly diminished (Fig. 11). In the case of low sedimentation rate, only in Model 1 is there a slight change with no growth stratal offlap developed in the forelimb (Fig. 12).

DISCUSSION

The geometric models for detachment growth folds described above show how fold kinematics, deformation mechanisms and sedimentation rates dramatically affect the growth stratal architectures of these fault-related fold systems. The models presented in this paper illustrate the first-order fundamental relationships of detachment growth systems. In nature one might expect, however, that rounded-hinge folding, variations in shortening and sedimentation rates, local erosion and redeposition, particular sedimentary facies and depositional patterns (e.g. hemipelagic drape, deposition on slopes), and sediment compaction would modify the stratal patterns demonstrated in this paper. Such features, however, require more complex interactive algorithms to simulate such detachment growth fold complexities and are beyond the scope of the present study. Given the limitations of the simple models presented in this paper, many of the results presented here show significant differences in growth stratal architectures, indicating that in some cases it may be possible to distinguish different kinematic models for detachment fold evolution. Unfortunately, some key features to distinguish between different kinematic models occur in crestal regions of anticlines, yet these geometries are unlikely to be found in some tectonic regimes where erosion would remove the record. It must also be noted that the models presented in this paper were calculated using a particular combination of parameters for the development of a single asymmetric detachment anticline above a layer-parallel detachment fault tip. It is possible to use many other values of competent layer thickness, ductile layer thickness, backlimb/forelimb length ratios, forelimb and backlimb dips, shortening and uplift to model detachment growth folds, resulting in a wide variety of detachment fold styles and hence a wide range of growth stratal architectures. In this paper we have used a moderately asymmetric detachment fold without an overturned forelimb as typical of many simple detachment fold systems (Homza and Wallace, 1995; Poblet and McClay, 1996).

Under conditions of high syntectonic sedimentation rates, the different models of detachment fold kinematics produce different growth stratal architectures. Model 1 produces a buried anticline with fanning growth patterns on both limbs (Fig. 3), with the differential rotation being most pronounced on the forelimb, thus permitting determination of fold asymmetry and vergence. In some circumstances, at high values of shortening, it may be possible to develop the unusual geometry of a syncline on top of the anticlinal crest. Model 2 growth stratal patterns under conditions of high syntectonic sedimentation do not produce fan structures but rather the growth stratal boundaries parallel those in the pre-growth units (Fig. 4). Growth strata above the crest of the anticline remain flat throughout the whole evolution. Model 3 growth folds formed under high sedimentation rates typically show fanning growth patterns in the upper part of the anticline as a result of limb rotation, but growth strata parallel the pre-growth units in the lower part as a result of hinge migration (Fig. 5). In a manner

similar to that for Model 1 folds, Model 3 folds may also form a syncline in growth units above the crest of the detachment anticline and an asymmetric pattern which allows determination of fold vergence. These may be very difficult to differentiate from Model 1 growth folds formed under similar conditions.

Models 1, 2 and 3 also produce different growth architectures under conditions of low sedimentation rates, Model 1 produces fanning growth structures ('progressive unconformities' of Riba, 1976) on both limbs of the fold (Fig. 6). The forelimb growth fan, however, is more pronounced and may be used to indicate fold/fault vergence. In contrast, Models 2 and 3 produce growth strata that are carried onto the fold limbs as the layers are fed through the active axial surfaces (Figs 7 & 8).

Given the limitations of the models presented there are a number of features of the growth strata in the models that are first order predictions likely diagnostic of detachment fold kinematics. Thus, when limb rotation occurs there are fanning growth structures consisting of beds progressively thinning towards the fold crest and decreasing in dip upwards, distinctive backlimb and forelimb geometries, and crestal synclines when syntectonic sediments overlap the anticlines. In contrast, when material is fed through the axial surfaces the growth stratal boundaries are parallel to the pre-growth fold limbs so that growth strata consist of panels of rocks with constant dip and thinning over the fold crest, no marked asymmetry develops between the forelimb and backlimb, and the growth strata above the anticline crest remain flat-lying. Under high sedimentation rates a combination of some of these features occurs where both limb rotation and hinge migration take place. In contrast, under low sedimentation rates growth stratal patterns associated with folds formed by limb rotation and hinge migration show basically the same features as folds formed by hinge migration. The effects of different deformation mechanisms on growth stratal architectures show that shear parallel to the pre-growth layers appears to generate only very minor differences compared to flexural slip mechanisms. In contrast, vertical shear markedly thins and increases the dip of forelimb growth strata when limb rotation occurs. Moreover, the amplitude of the growth syncline on the crest of the anticlines is markedly diminished.

It is important to note that some patterns shown in the models are highly dependent on factors other than the fold kinematics. For instance, in our models we have assumed constant sedimentation and shortening rates, however, varying either (or both) of these rates will result in different onlap–offlap–overlap geometries. Because such varying rates occur in natural examples (Rowan *et al.*, 1993), the usefulness of the onlap–offlap–overlap patterns displayed in our models is restricted to specific situations in which constant rates apply. Additionally, the adoption of a kink-fold geometry for modelling purposes creates abrupt dip changes in the sediments. A large number of natural folds show rounded geometries (see for instance the natural examples described below) which would result in smooth boundaries between dip domains in the growth strata. Similar considerations regarding the detailed geometries, thicknesses and dips of the growth strata can be made when the influence of local erosion, particular sediment facies, deposition on slopes, compaction, etc. are taken into account. However, the effect of those parameters in the growth stratal patterns should be tested by applying a more complex modelling procedure.

The viability of theoretical models presented above need to be tested against natural examples of detachment growth folds.

Natural examples of detachment growth folds

The fold–thrust belt of the southern Pyrenees in Spain displays many spectacular growth fault-related fold relationships (Puigdefàbregas, 1975; Riba, 1976; Nichols, 1987; Specht *et al.*, 1991; Mellere, 1993; Millán *et al.*, 1994; Burbank and Vergés, 1994; Poblet and Hardy, 1995 and others). In particular, many of the growth folds that are developed above the Triassic evaporitic sequences of the central western and southwestern Pyrenees may be interpreted as detachment folds. Two such anticlines, the Mediano anticline in the Ainsa Basin, and the Pico de Aguila anticline in the External Sierras (Fig. 13) have been interpreted as detachment growth folds (Holl and Anastasio, 1993; Poblet and Hardy, 1995). Here we compare the growth stratal architectures of the Mediano and Pico de Aguila anticlines with the geometric models of detachment growth folds described above. No attempt has been made to model these particular examples because they show some features not considered in our theoretical models (rounded-hinge folds, possible variations in the shortening rate, facies deposited on slopes, compaction). Nevertheless, they contain a number of the key features seen in the detachment growth fold models, which allow us to be precise about their kinematics.

Figure 14(a) shows a cross-section of the Mediano anticline in the Southern Pyrenees, Spain. This probably developed as a detachment fold (Holl and Anastasio, 1993) formed by a thick, competent pre-growth package of Upper Cretaceous to Cuisian limestones and sandstones detached over Triassic shales with intercalated limestones and evaporites. The growth strata consist of Lutetian to Bartonian shales, limestones and sandstones (Fig. 14b). Unpublished studies in progress using additional biostratigraphic and palaeomagnetic data allowed us to ascertain that the rate of sedimentation was approximately constant during fold growth. The older growth strata onlap the Mediano anticline, whereas the younger growth strata overlap the anticlinal crest. These relationships indicate that the fold uplift rate was greater than the sedimentation rate during the initial phase of

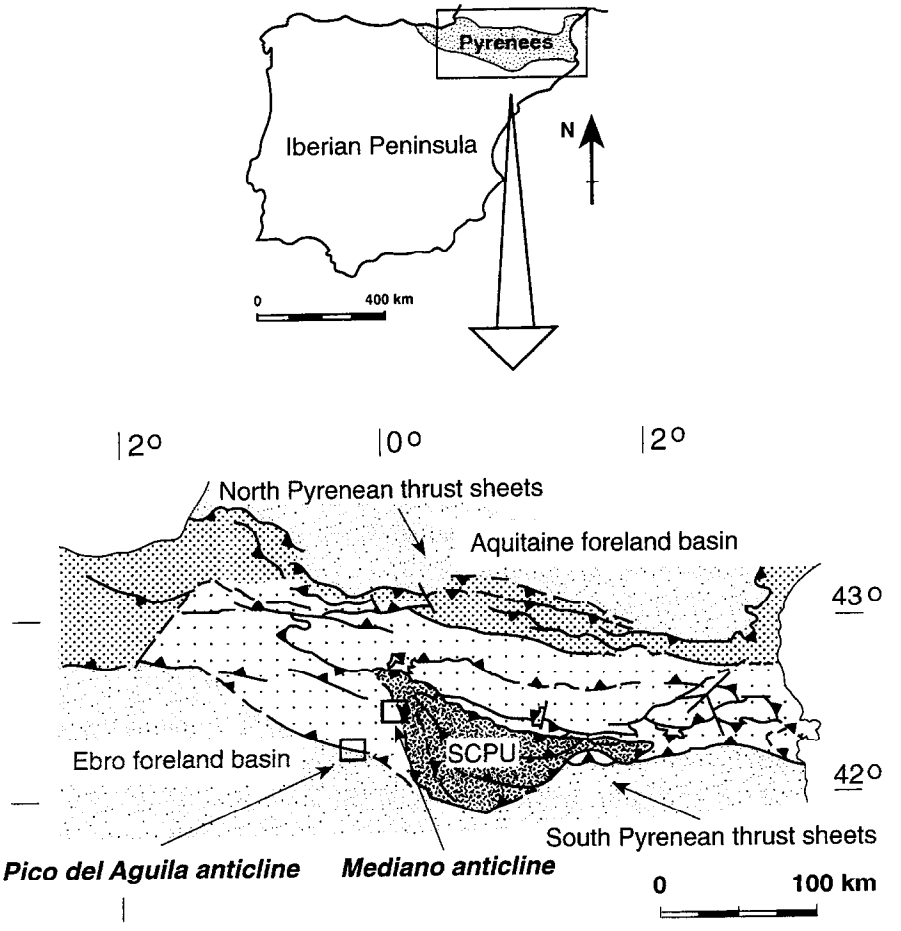

Fig. 13. Tectonic map of the Spanish Pyrenees showing the location of the Mediano and Pico de Aguila detachment anticlines (Figs 14 & 15).

fold amplification. During this time, noticeable anticline crestal erosion and redeposition of the eroded material in the adjacent basins occurred, allowing the younger growth strata to overlap the anticline (Fig. 14). Despite this discrepancy between the natural example and our theoretical models that do not incorporate erosion, there are some geometric similarities between the asymmetric Mediano anticline structure and the kinematic models described above. The Mediano growth strata show fanning wedge geometries on both limbs that form well-constrained progressive unconformities (Fig. 14). In addition, on the backlimb of the Mediano anticline the distinctive Lutetian reefal unit onlaps the pre-growth beds, whereas it partially overlaps the eroded crest in the forelimb (Fig. 14). From these geometrical relationships it is possible to interpret the Mediano anticline as either a Model 1 or Model 3 detachment fold with growth stratal architectures similar to those shown in Figs 3 and 5. Assuming that presently observed spatial variations in the Mediano anticline geometry are equivalent to geometric variations in time we conclude that the anticline formed with variable limb length and limb dip. Limb rotation was the main folding mechanism accompanied by minor hinge migration.

The Pico del Aguila anticline, Southern Pyrenees, Spain (Fig. 15) is a superbly exposed symmetric detachment growth fold (Puigdefàbregas, 1975; Barnolas *et al.*, 1992; Millán *et al.*, 1994; Poblet and Hardy, 1995). It is formed by a pre-growth sequence of competent Upper Cretaceous to Upper Lutetian limestones and sandstones detached on a unit of Triassic shales intercalated with limestones and evaporites. Growth strata comprise Upper Lutetian to Priabonian shales and sandstones that form a well exposed fanning growth wedge on both limbs of the structure (Fig. 15a). Rates of syntectonic sedimentation associated to the Pico del Aguila anticline were approximately constant (Poblet and Hardy, 1995). The older growth strata onlap both limbs of the anticline whereas younger growth units overlap the anticlinal crest (Fig. 15). The growth strata display spectacular progressive unconformities on both anticline limbs, i.e. the syntectonic sediments decrease in dip up-section and thin towards the anticline crest and no erosive truncations between growth strata have been recognised (Fig. 15) (Puigdefàbregas, 1975; Barnolas *et al.*, 1992; Millán *et al.*, 1994; Poblet and Hardy, 1995). The growth stratal architecture displayed by the Pico de Aguila anticline is comparable to those found in either Model 1 or Model 3

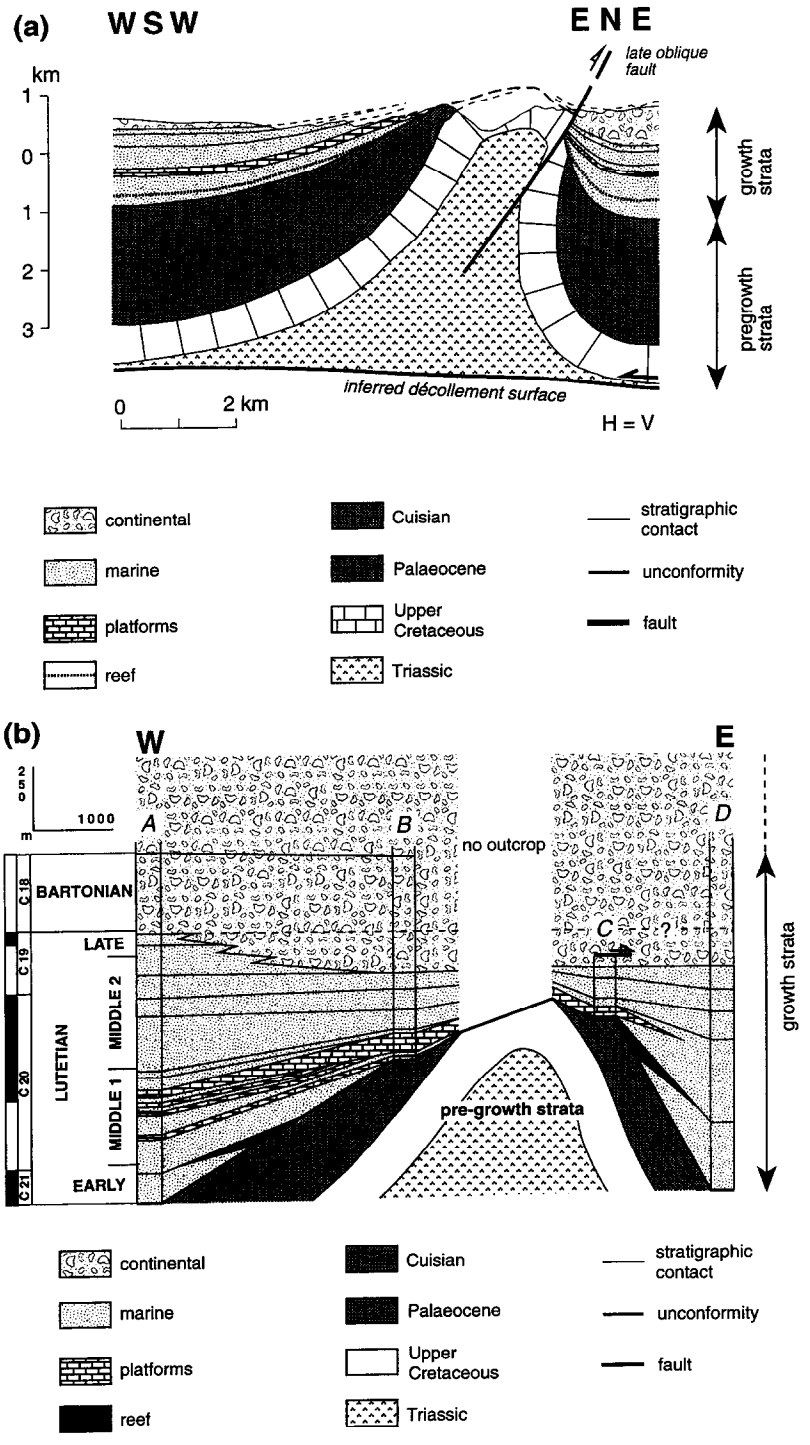

Fig. 14. Cross-section through the southern part of the Mediano Anticline, Ainsa Basin, Southern Pyrenees, Spain (a), and correlation of four stratigraphic sections (A, B, C and D) showing growth strata (b) derived from field mapping by J. Poblet, J. A. Muñoz, A. Travé and J. Serra-Kiel. The relationships between the growth and pre-growth strata, and the location of the cross-sections with respect to the anticline are illustrated.

detachment growth folds formed by flexural slip mechanisms under conditions of high syntectonic sedimentation rates (Figs 3 & 5). Extensional faulting at the crest of the anticline may have obscured any syncline that might have developed in this position. Poblet and Hardy (1995) concluded that several deformation mechanisms (including flexural slip, shearing parallel to pre-growth strata, hinge thickening and cleavage development) were operative during the growth of the Pico de Aguila anticline, thus producing a growth stratal architecture that does not exactly match those of Model 1 in Fig. 3 or Model 3 in Fig. 5.

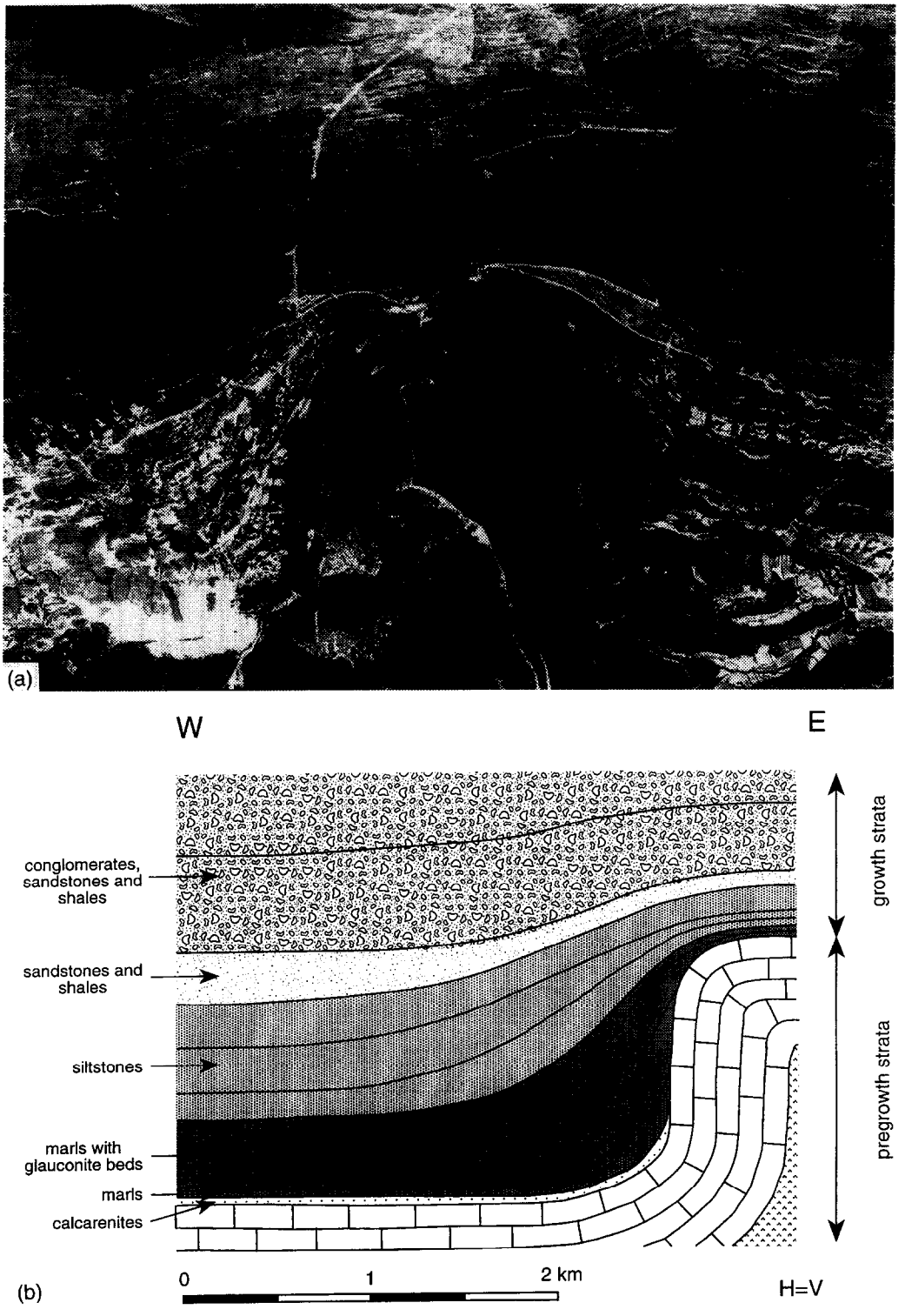

Fig. 15. Aerial photograph of the Pico del Aguila anticline, External Sierras, Southern Pyrenees, Spain (a), and down-dip cross-section of the western limb of the anticline (b). North is on the upper side of the photograph. The pre-growth strata correspond to the dark coloured area in the lower central part of the photograph. The lower growth strata onlap on the anticline limbs, whereas the upper growth strata overlap and thin dramatically over the anticline crest. The approximate size of the photographs is 9.8 × 9.8 km. Modified from Poblet and Hardy (1995).

CONCLUSIONS

The comparative kinematics of the three models for single layer detachment folds involving a competent unit with constant bed length and thickness indicate that the growth stratal geometries depend on axial surface activity, limb rotation, limb lengthening, uplift rate, deformation mechanisms within the syntectonic sediments, and sedimentation rate. For the same finite fold shape in the pregrowth units and the same shortening and sedimentation rates, different patterns in the growth strata are obtained for different detachment folding kinematics. Given the simplistic assumptions (kink geometry, constant shortening and sedimentation rates, sediments deposited horizontally, no erosion and no compaction) the geometries of the syntectonic sediments may be used to infer the kinematics of detachment folds — they act as a 'tectonic tape recorder' preserving a record of progressive fold development. In addition, some of the models of growth stratal geometries exhibit noticeable differences between forelimbs and backlimbs and hence indicate fold/fault vergence. As a consequence, in areas of poor seismic imaging or where only the growth strata are exposed they may be good indicators of structural vergence.

When growth strata are deformed by flexural slip, limb rotation produces fanning growth structures consisting of beds decreasing in dip up-section and thinning progressively towards the fold crest. In contrast, hinge migration leads to panels of rocks with constant dip largely parallel to the pre-growth beds and thinning over the anticline crest. Shear parallel to the pre-growth strata produces hardly any modification of the growth geometries, whereas vertical shear causes thinning and increasing in dip of the forelimb growth strata.

The Mediano and Pico de Aguila detachment anticlines in the southern Spanish Pyrenees show syntectonic growth architectures very similar to the theoretical Model 1 or Model 3 detachment folds formed under conditions of high sedimentation rates. Our results demonstrate that careful analysis of detachment fold growth patterns may give us a better understanding of the kinematic histories of natural detachment fold systems.

Acknowledgements—We thank Donald Fisher, Mark G. Rowan and Rob Butler for their suggestions which have improved this manuscript. J. Poblet acknowledges the Commission of the European Communities (Human Capital and Mobility Fellowship 1993–95) and the Generalitat de Catalunya (Beca de Reincorporació de Doctors a Centres de Recerca i Universitats Públiques Catalanes 1995–97) (Grup de Recerca: Geodinàmica i Anàlisi de Conques) for their financial support. F. Storti thanks the Italian M.U.R.S.T. (Grants to F. Salvini). This study is part of the Fault Dynamics Project sponsored by ARCO British Ltd, BP Exploration, PETROBRAS UK Ltd, CONOCO UK Ltd, MOBIL North Sea Ltd and SUN Oil Britain to whom we are grateful. The Spanish Ministry for Education and Science (Beca Postdoctoral en el Extranjero 1992–93), the Ainsa Basin Project (1992–93) funded by Norsk Hydro a.s. and the Integrated Basin Studies Project (1993–95) funded by the Commission of the European Communities are gratefully acknowledged for their financial support during part of the field seasons. Fault Dynamics Publication No. 63.

REFERENCES

Barnolas, A., Teixell, A., Samsó, J. M. and Zamorano, M. (1992) Estructura y evolución sedimentaria del sector central de la cuenca surpirenaica. III Congresso de Geologia de España, Salamanca, 1992. *Excursiones* **1**, 74–114.

Beutner, E. C. and Diegel, F. A. (1985) Determination of fold kinematics from syntectonic fibers in pressure shadows, Martinsburg slate, New Jersey. *American Journal of Science* **285**, 16–50.

Burbank, D. W. and Vergés, J. (1994) Reconstruction of topography and related depositional systems during active thrusting. *Journal of Geophysical Research* **99**, 20281–20297.

Dahlstrom, C. D. A. (1990) Geometric constraints derived from the law of conservation of volume and applied to evolutionary models for detachment folding. *Bulletin of the American Association of Petroleum Geologists* **74**, 336–344.

De Sitter, L. V. (1956) *Structural Geology*. McGraw-Hill, New York.

Fischer, M. P., Woodward, N. B. and Mitchell, M. M. (1992) The kinematics of break thrust folds. *Journal of Structural Geology* **14**, 451–460.

Hardy, S. and Poblet, J. (1994) Geometric and numerical model of progressive limb rotation in detachment folds. *Geology* **22**, 371–374.

Hardy, S. and Poblet, J. (1995) The velocity description of deformation. Paper 2: sediment geometries associated with fault-bend and fault-propagation folds. *Marine and Petroleum Geology* **12**, 165–176.

Hardy, S., Poblet, J., McClay, K. and Waltham, D. (1996) Mathematical modelling of growth strata associated with fault-related fold structures. *Special Publication of the Geological Society* **99**, 265–282.

Holl, J. E. and Anastasio, D. J. (1993) Paleomagnetically derived folding rates, Southern Pyrenees, Spain. *Geology* **21**, 271–274.

Homza, T. X. and Wallace, W. K. (1995) Geometric and kinematic models for detachment folds with fixed and variable detachment depths. *Journal of Structural Geology* **17**, 575–588.

Jamison, W. R. (1987) Geometric analysis of fold development in overthrust terranes. *Journal of Structural Geology* **9**, 207–219.

Mellere, D. (1993) Thrust-generated, back-fill stacking of alluvial fan sequences, south central Pyrenees, Spain (La Pobla de Segur conglomerates). *Special Publication of the International Association of Sedimentology* **20**, 259–276.

Millán, H., Aurell, M. and Melendez, A. (1994) Synchronous detachment folds and coeval sedimentation in the Pre-Pyrenean External Sierras (Spain): a case study for a tectonic origin of sequences and system tracts. *Sedimentology* **5**, 1001–1024.

Mitchell, M. M. and Woodward, N. B. (1988) Kink detachment fold in the southwest Montana fold and thrust belt. *Geology* **16**, 162–165.

Nichols, G. J. (1987) Syntectonic alluvial fan sedimentation, southern Pyrenees. *Geological Magazine* **124**, 121–133.

Poblet, J. and Hardy, S. (1995) Reverse modelling of detachment folds; application to the Pico del Aguila anticline in the south central Pyrenees (Spain). *Journal of Structural Geology* **17**, 1707–1724.

Poblet, J. and McClay, K. (1996) Geometry and kinematics of single layer detachment folds. *Bulletin of the American Association of Petroleum Geologists* **80**, 1085–1109.

Puigdefàbregas, C. (1975) La sedimentación molásica en la cuenca de Jaca. *Pirineos* **104**, 1–108.

Riba, O. (1976) Syntectonic unconformities of the Alto Cardener, Spanish Pyrenees: a genetic interpretation. *Sedimentary Geology* **15**, 213–233.

Rowan, M. G., Kligfield, R. and Weimer, P. (1993) Processes and rates of deformation: preliminary results from the Mississippi fan foldbelt, deep gulf of Mexico. *GCSSEPM Foundation 14th Annual Research Conference*, pp. 209–218.

Specht, M., Déramond, J. and Souquet, P. (1991) Relations tectonique–sédimentation dans les bassins d'avant-pays: utilisation des surfaces stratigraphiques isochrones comme marqueurs de la déformation. *Bulletin de la societé géologique* **162**, 553–562.

Suppe, J., Chou, G. T. and Hook, S. C. (1992) Rates of folding and faulting determined from growth strata. In: *Thrust Tectonics*, ed. K. R. McClay, pp. 105–121. Chapman and Hall, London.

Torrente, M. M. and Kligfield, R. (1995) Modellizzazione predittiva di pieghe sinsedimentarie. *Bolletino de la Società Geologica Italiana* **114**, 293–309.